1. ALMA observations

The Atacama Large Millimetre/submillimetre Array (ALMA) began operations in September 2011 in its Early Science configuration. During the Cycle 0 observing period, ALMA offered observations with 16 12m antennas, in a compact (baselines up to 200m) and extended configuration (with baselines up to 450m). Four frequency bands were offered (bands 3, 6, 7, and 9 at 100, 245, 325, and 660 GHz, respectively). Already in this early configuration ALMA was one of the most sensitive interferometers of its kind.

For Cycle 0 we proposed to observe the detached shell around R Sculptoris in bands 3, 6, and 7, targeting the $CO(J = 1 - 0)$, $CO(J = 2 - 1)$, and $CO(J = 3 - 2)$ emission lines (project ID ADS/JAO.ALMA#2011.0.00131.S). The spectral setup also allowed us to observe the $CN(N = 1 - 0)$ (band 3), $SiO(J = 5 - 4)$ (band 6), and $^{13}CO(J = 3 - 2)$, $H^{13}CN(J = 4 - 3)$, and $CS(J = 7 - 6)$ (band 7) lines. The first set of data was delivered to the European ALMA Regional Centre (ARC) in December 2011, after having passed quality assurance by the Joint ALMA Observatory (JAO). Here we present the results of the $CO(J = 3 - 2)$ observations in band 7. The full observations will be presented in a forthcoming paper.

The band 7 data was taken on October 3-4 and 18-19 in 2011 in the compact configuration. Four spectral windows of 1.875 GHz and 3840 channels were tuned at 345.1 GHz, 343.3 GHz, 331.1 GHz, and 333.0 GHz covering the $CO(J = 3 - 2)$ line at 345.795 GHz, as well as the $^{13}CO(J = 3 - 2)$ (330.587 GHz), $H^{13}CN(J = 4 - 3)$ (345.340 GHz), and $CS(J = 7 - 6)$ (342.882 GHz) lines.

The entire shell around R Sculptoris was covered in a 45-point mosaic, covering a region of 50"×50". The beam of the $CO(J = 3 - 2)$ observations is 1.3"×1.0" with a position angle of 91 degrees. The total observing time (including calibrations) was ≈6 hours.

The data were reduced using the Common Astronomy Software Application (CASA) package. Initial calibration consisted of applying phase corrections based on water vapour radiometer monitoring and improved antenna positions as well as a manual delay calibration. Subsequent bandpass calibration was performed on the quasar 3C454.3. Amplitude calibration was done bootstrapping from Neptune to the phase calibrator J0137-245 and finally the amplitude and phase calibration solutions determined on J0137-245 were applied to R Sculptoris. Imaging was done using the CASA clean algorithm on the data that was smoothed to a $0.5 \, \text{km s}^{-1}$ velocity resolution. The noise level in the reduced data cube is 44mJy/beam.

2. The connection between thermal pulses and detached shells

A connection between thermal pulses and detached shells was postulated with the first discovery of a thin shell of gas around the carbon star S Sct[1]. A survey of all carbon stars within 600pc finds that ≈10% of all sources show detached shells in CO emission. The lifetime of an expanding, thin shell of CO is estimated to be ≈10,000 years. With an inter-pulse time of

≈100,000 years, the statistics are consistent with a scenario where detached shells are created due to the high mass-loss rate during a thermal pulses[2,3]. Finally, hydrodynamical models show that it indeed is possible to create a thin, expanding shell of gas due to the increase in mass-loss rate and expansion velocity during a thermal pulse[4,5]. In order to form the shell, a sufficiently high increase in expansion velocity is required. Variations in the expansion velocity between thermal pulses are generally small $(1 - 2 \, \text{km s}^{-1})^4$, and are not sufficient to form the observed detached shells. The increase in luminosity during a thermal pulse increases the radiation pressure on the dust grains, and hence the expansion velocity of the wind. It is hence likely that the observed detached shells of gas around carbon stars are due to the variation in mass-loss rate and expansion velocity during a thermal pulse.

3. Measurement of the velocity and mass-loss rate evolution

The derived evolution of the expansion velocity depends strongly on the derived period of the binary system. Figure 2 shows that the first 2.5 windings are nearly parallel. The distance between the fit to the peak intensities of the observed emission over these windings is 2.6"±0.07" (corresponding to 1.13×10^{16} cm $\pm 0.3 \times 10^{16}$ cm at a distance of 290 pc). Assuming the present-day expansion velocity (determined from modelling of HCN emission lines[6]) then gives a period of 350±10 years. The size of the HCN envelope is on the order of 10^{16} cm. At $10.5 \, \text{km s}^{-1}$ it will take material on average ≈300 years to reach the outer HCN envelope. The HCN emission hence probes a region that covers timescales that are larger than the velocity variations seen in the ALMA observations, and will measure an average expansion velocity over this region. We therefore conclude that the expansion velocity measured by the HCN emission lines is a good estimate also of the average expansion velocity during the last 2.5 binary periods.

In order to determine the expansion velocity and radius of the shell we measured the projected size of the shell in each velocity channel (Fig. S1). The radius was determined by taking an azimuthally averaged radial profile centred on the stellar position. A fit assuming a spherically symmetric shell expanding at constant velocity results in a shell size of $R_{sh}=18.5$", expanding at a velocity of $v_{sh}=14.3\pm0.5 \, \text{km s}^{-1}$.

The total mass in the shell is estimated to be $2.5 \times 10^{-3} \, M_\odot$, based on modelling of ^{12}CO emission lines[6]. The mass-loss rate during the pulse is determined by the pulse duration. An upper limit to the pulse duration is set by the binary period to 350 years, in order to create a spherical shell that is not shaped by the binary system. The shell is marginally resolved with the 1.3"×1.0" ALMA beam . For a velocity of $14.3 \, \text{km s}^{-1}$ and a distance of 290 pc this sets a lower limit to the pulse duration of 100 years. The resulting pulse mass-loss rate is hence between $7 \times 10^{-6} \, M_\odot \, \text{yr}^{-1}$ and $2.5 \times 10^{-5} \, M_\odot \, \text{yr}^{-1}$. The mass-loss rate before and after the pulse will affect the ratio between the peak emission in the spiral structure and in the shell. Since we detect no spiral outside of the detached shell, this sets an upper limit to the mass-loss rate before the pulse. However, the lack of observations of molecular gas outside the detached shell may also be an excitation effect, and/or the dissociation of CO due to the interstellar UV radiation field. Similarly, the CO emission depends on the circumstellar chemistry and the details of
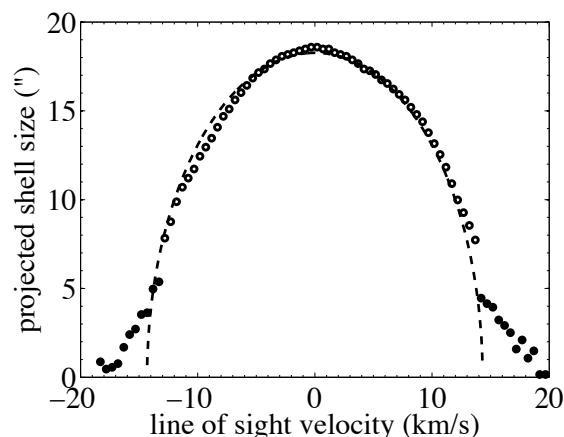
Supplementary Figure 1: Projected shell size vs. line of sight velocity (relative to the stellar velocity). The size of the detached shell is measured in radial profiles averaged over all position angles for each velocity channel. The open circles points show measurements where the detached shell can be clearly separated from other structure, while at extreme velocities (filled circles) different structures merge together. The dashed line shows a fit to the open circles assuming a spherically symmetric shell expanding at a constant velocity. The fit gives a shell size of 18.5" and expansion velocity of $14.3\,\mathrm{km\,s^{-1}}$.

the radiative excitation, and may hence not translate directly into a total density distribution. An additional uncertainty is the possibility that flux is resolved-out due to missing zero-spacing observations. Single-dish observations of R Sculptoris with the Atacama Pathfinder Experiment (APEX) indicate that indeed some extended flux is missed in the ALMA data. However, the pre-pulse mass-loss should have been shaped into a spiral by the binary companion, hence leading to structures on size-scales that would be detected in our ALMA observations. Likewise, the evolution of the mass-loss rate after the thermal pulse is constrained by the contrast between the spiral windings and the inter-winding medium, and may be affected by resolution effects on large scales. The effect of resolved-out flux will be discussed in detail in a forthcoming publication with the complete data. The present-day mass-loss rate is based on models of HCN emission lines[6]. Although the value depends on the ratio of HCN to H_2, these observations have the advantage of only probing the present-day wind, hence the fitting of the emission lines is not complicated by emission from the detached shell.

The derived binary separation is 60 AU, and the companion will not affect the thermal pulse properties of R Sculptoris itself, but only on the shaping of the wind. The derived thermal pulse properties are hence also valid for single stars.
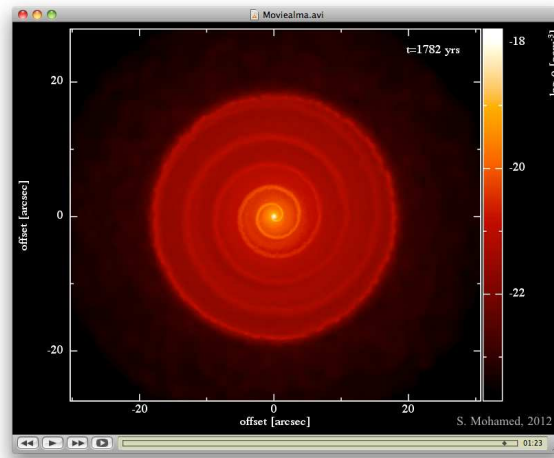
Supplementary Movie: Animation of the SPH model of the evolution of the CSE around R Sculptoris over 2,200 years. We model a binary system in which the AGB star undergoes a thermal pulse. The mass of R Sculptoris is assumed to be $1.6\,M_\odot$[7], and the observed density contrast in the inner windings indicates a companion mass of $0.25\,M_\odot$[18]. A circular orbit and the derived orbital period yield a binary separation of 60 AU. The evolution of the expansion velocity is derived directly from the observations. Wind particles are injected at the surface of the AGB star at the mass-loss rate shown in Figure 3. The shaping of the wind into a spiral structure is clearly visible. At t=0 years the AGB star undergoes a thermal pulse, forming an expanding detached shell. The post-pulse mass-loss continues to form a spiral, connecting the detached shell with the central star. At t≈2,000 years the system has formed a detached shell and spiral structure as observed in the ALMA observations. The observed structure depends on the inclination angle of the binary system to the line of sight, which is 90º in this animation. However, a full spiral structure will be observed up to inclination angles of 20-30º to the line of sight.

4. 3-dimensional hydrodynamical and radiative transfer models

We modelled a binary system with a separation of 60 AU and primary and companion masses of $1.6\,M_\odot$[7] and $0.25\,M_\odot$, respectively. The model uses smoothed particle hydrodynamics (SPH), a Lagrangian method in which particles represent the fluid[8,9,10]. We use the GADGET-2 SPH code in which the momentum equation is derived based on an entropy formulation which conserves entropy, energy, and momentum by construction[11]. Viscosity terms to capture shocks and self-gravity of the gas are also included[12]. The particles have adaptive smoothing lengths and are evolved with individual and adaptive time steps for better and more efficient spatial and time resolution. We include cooling and heating by, e.g., rotational and vibrational transitions of H_2, CO and H_2O, H_2 dissociative cooling and reformation heating, gas-grain cooling/heating, and an atomic cooling function that includes non-equilibrium effects[13,14].

The results from the SPH simulations were used as an input for the 3-dimensional radiative transfer modelling with LIME, a flexible, non-LTE line excitation and radiation transfer method for millimeter and far-infrared wavelengths[15]. We assumed a constant abundance of CO relative to H_2 of 1×10^{-3} (typical for carbon stars[16,17]). The SPH results were gridded to a 40 AU resolution, which in turn was extrapolated onto the Voronoi grid. The temperature, density, and velocity were taken directly from the SPH models, assuming a $0.6 \, \mathrm{km \, s^{-1}}$ turbulent line width. The radiative transfer was calculated using the lowest 40 energy levels of CO.

References

1. Olofsson, H., Eriksson, K. & Gustafsson, B. SEST CO (J = 1 - 0) observations of carbon-rich circumstellar envelopes. *A&A* **196**, L1–L4 (1988).

2. Olofsson, H., Carlstrom, U., Eriksson, K., Gustafsson, B. & Willson, L. A. Bright carbon stars with detached circumstellar envelopes - A natural consequence of helium shell flashes? *A&A* **230**, L13–L16 (1990).

3. Olofsson, H., Eriksson, K., Gustafsson, B. & Carlstrom, U. A study of circumstellar envelopes around bright carbon stars. I - Structure, kinematics, and mass-loss rate. *ApJS* **87**, 267–304 (1993).

4. Mattsson, L., Höfner, S. & Herwig, F. Mass loss evolution and the formation of detached shells around TP-AGB stars. *A&A* **470**, 339–352 (2007).

5. Steffen, M. & Schönberner, D. On the origin of thin detached gas shells around AGB stars. Insights from time-dependent hydrodynamical simulations. *A&A* **357**, 180–196 (2000).

6. Schöier, F. L., Lindqvist, M. & Olofsson, H. Properties of detached shells around carbon stars. Evidence of interacting winds. *A&A* **436**, 633–646 (2005).

7. Claussen, M. J., Kleinmann, S. G., Joyce, R. R. & Jura, M. A flux-limited sample of Galactic carbon stars. *ApJS* **65**, 385–404 (1987).

8. Rosswog, S. Astrophysical smooth particle hydrodynamics. *NewAR* **53**, 78–104 (2009).

9. Springel, V. Smoothed Particle Hydrodynamics in Astrophysics. *ARA&A* **48**, 391–430 (2010).

10. Price, D. J. Smoothed particle hydrodynamics and magnetohydrodynamics. *Journal of Computational Physics* **231**, 759–794 (2012).

11. Springel, V. The cosmological simulation code GADGET-2. *MNRAS* **364**, 1105–1134 (2005).

12. Barnes, J. & Hut, P. A hierarchical O(N log N) force-calculation algorithm. *Nature* **324**, 446–449 (1986).

13. Smith, M. D. & Rosen, A. The instability of fast shocks in molecular clouds. *MNRAS* **339**, 133–147 (2003).

14. Mohamed, S., Mackey, J. & Langer, N. 3D simulations of Betelgeuse's bow shock. *A&A* **541** (2012).

15. Brinch, C. & Hogerheijde, M. R. LIME - a flexible, non-LTE line excitation and radiation transfer method for millimeter and far-infrared wavelengths. *A&A* **523**, A25 (2010).

16. Ramstedt, S., Schöier, F. L., Olofsson, H. & Lundgren, A. A. On the reliability of mass-loss-rate estimates for AGB stars. *A&A* **487**, 645–657 (2008).

17. De Beck, E. *et al*. Probing the mass-loss history of AGB and red supergiant stars from CO rotational line profiles. II. CO line survey of evolved stars: derivation of mass-loss rate formulae. *A&A* **523** (2010).

18. Kim, H. & Taam, R. E. Probing Substellar Companions of Asymptotic Giant Branch Stars through Spirals and Arcs. *ApJ* **744**, 136 (2012).